Electronic Supplementary Material (ESI) for Inorganic Chemistry Frontiers.
This journal is © the Partner Organisations 2023

Supporting Information

1 Experimental Section

1.1 Preparation of Acetate Ions-Intercalated $Ni_{0.7}Co_{0.3}$-LDH and other LDHs

Firstly, 174.2 mg (0.7 mmol) of nickel acetate tetrahydrate and 74.7 mg (0.3 mmol) of cobalt acetate tetrahydrate were dispersed into the 20 mL methanol, ultrasonic for 30 min to dissolve the metal salt completely. Then the solution was transferred into a 50 mL Teflon lining sealed in a stainless-steel shell and heated at 120 °C for 72 h. After cooling to room temperature, the precipitate was washed by centrifugation with water and ethanol for 3 times separately, 8000 rpm for 5 mins per time, to remove unreacted metal salts and unstable intercalated acetate ions. The product was dried in a vacuum oven at 60 °C for 24 h and collected by grinding, which is named $Ni_{0.7}Co_{0.3}$-LDH. In order to compare the experiments, the total amount of metal salts was kept constant at 1 mmol, and other reaction conditions were kept unchanged, only the molar ratio of nickel acetate and cobalt acetate was changed for the synthesis of Ni-LDH, $N_{i0.5}Co_{0.5}$-LDH, $Ni_{0.3}Co_{0.7}$-LDH, and Co-LDH.

1.2 Material characterization

The morphology was observed through a scanning electron microscope (SEM, Hitachi, Regulus 8200) and transmission electron microscope (TEM, JEOL, JEM-2100Plus). Crystalline structure was detected by X-ray diffraction (XRD, Bruker, D2 PHASER). The chemical composition and chemical state of synthesized samples were estimated using Fourier transform infrared (FTIR, Shimadzu IRTracer-100) spectroscopy and X-ray photoelectron spectroscopy (XPS, PerkinElmer PHI-5700 ESCA System). The particle pore size distribution and specific surface area were calculated by the N_2 adsorption-desorption isotherms at 77 K (Quantachrome IQ2) using the Brunauer-Emmett-Teller (BET) and non-local density functional theory (NLDFT) methods. Thermal stability was evaluated throuth the thermogravimetric analysis (TGA) conducted on a thermal analysis instrument (Netzsch, TG-209F3) over temperature ranging from RT to 800 °C under a nitrogen atmosphere with a heating rate of 5 °C min^{-1}.

1.3 Electrochemical Measurements

Electrochemical measurements were conducted by a CHI660E electrochemical workstation. The CV, GCD, and EIS of samples were tested in the three-electrode system with a Hg/HgO reference electrode, platinum sheet counter electrode, and 6M KOH electrolyte. EIS measurements were carried out from 0.01 Hz to 100 kHz of the frequency range. Meanwhile, the as-prepared 75 wt.% NiCo-LDH as active materials, 20 wt.% conductive carbon black, and 5 wt.% polytetrafluoroethylene (PTFE) were uniformly mixed for the preparation of the working electrode, respectively. The loading mass of every electrode is 2.0 mg. The asymmetric supercapacitors (ASCs) were assembled using $Ni_{0.7}Co_{0.3}$-LDH electrode as positive electrode and activated carbon as negative electrode with 6M KOH solution electrolyte. The gravimetric specific capacitance (C_s, F g^{-1}), power density (P, W kg^{-1}) and energy density (E, Wh kg^{-1}) of $Ni_{0.7}Co_{0.3}$-LDH //AC were calculated based on the equation:

$$C_S = \frac{it}{m\Delta V} \tag{1}$$

$$E = \frac{1}{2} C_s (\Delta V)^2 = \frac{i\int V dt}{M * 3.6} \tag{2}$$

$$P = \frac{E}{t} * 3600 \tag{3}$$

Where i and t are the discharge current and discharge time, m means the loading mass of cathode active material. The ΔV represents the charging-discharging potential window. M represents the total active material loading mass of the positive electrode and negative electrode.

1.4 DFT calculation

Generalized gradient approximation with the Perdew-Burke-Ernzerhof functional (GGA-PBE) was used for the exchange-correlation energy calculations. The commercial version of the DMol3 program and spin-polarized calculations were applied to calculate the ionization energy. The commercial version of the CASTEP program and spin-polarized calculations were used for the calculation of the electron

density difference map and partial density of states (PDOS). The Brillouin zone was sampled by a Monkhorst-Pack grid as the Γ-point for all systems with 1 × 1 × 1 k-points. The self-consistent field (SCF) convergence for each electronic energy was set as 1.0×10^{-5} Ha, 0.002 Ha $Å^{-1}$ for force and 0.005 Å for displacement.

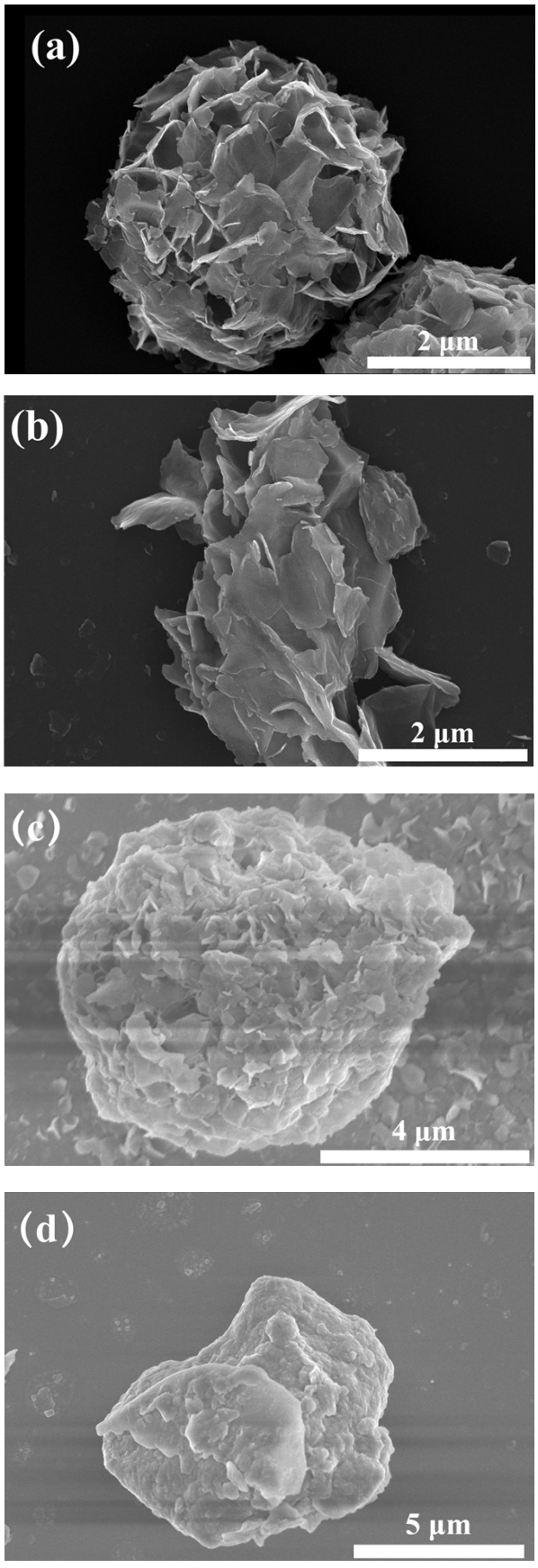

Fig. S1. SEM images of $Ni_{0.7}Co_{0.3}$-LDH synthesized in (a) 24 h and (b) 48 h. SEM images of synthesized (c) Ni-LDH and (d) Co-LDH.

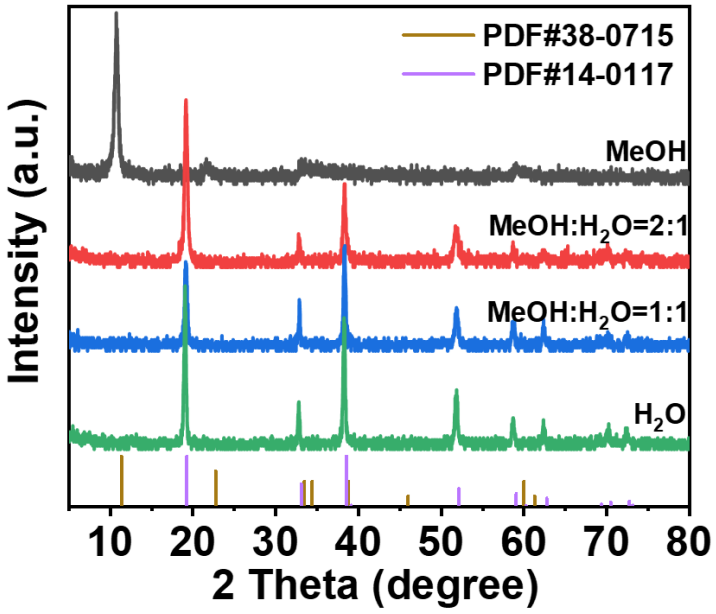

Fig. S2. XRD patterns of $Ni_{0.7}Co_{0.3}$-LDH synthesized in different solvents.

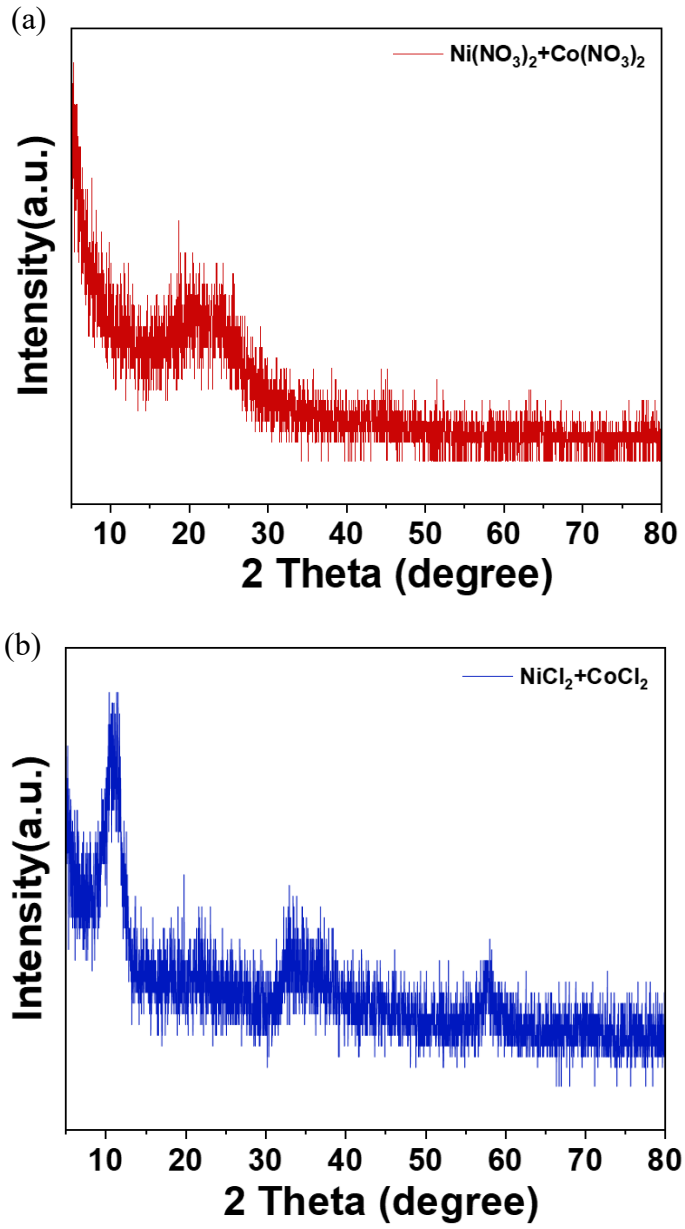

Fig. S3. XRD patterns of $Ni_{0.7}Co_{0.3}$-LDH synthesized by (a) nitrate and (b) chloride.

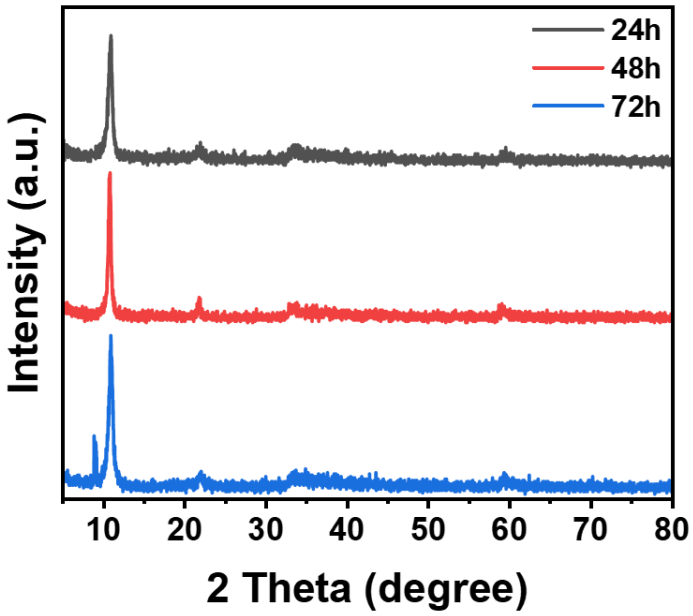

Fig. S4. XRD patterns of $Ni_{0.7}Co_{0.3}$-LDHs synthesized in different time.

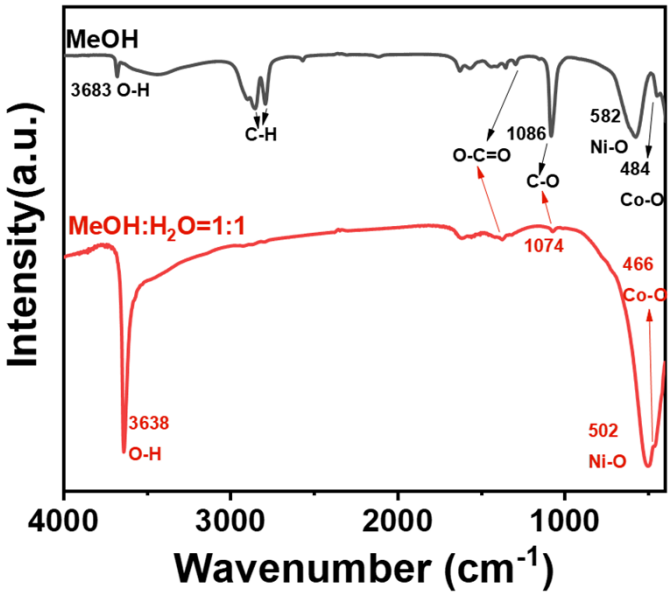

Fig. S5. FT-IR spectra of $Ni_{0.7}Co_{0.3}$-LDHs synthesized in different solvents.

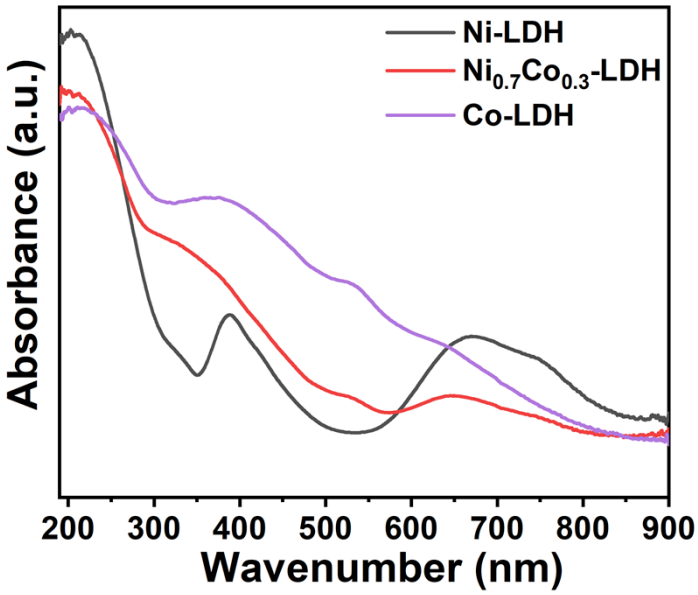

Fig. S6. UV-vis spectra of NiCo-LDHs.

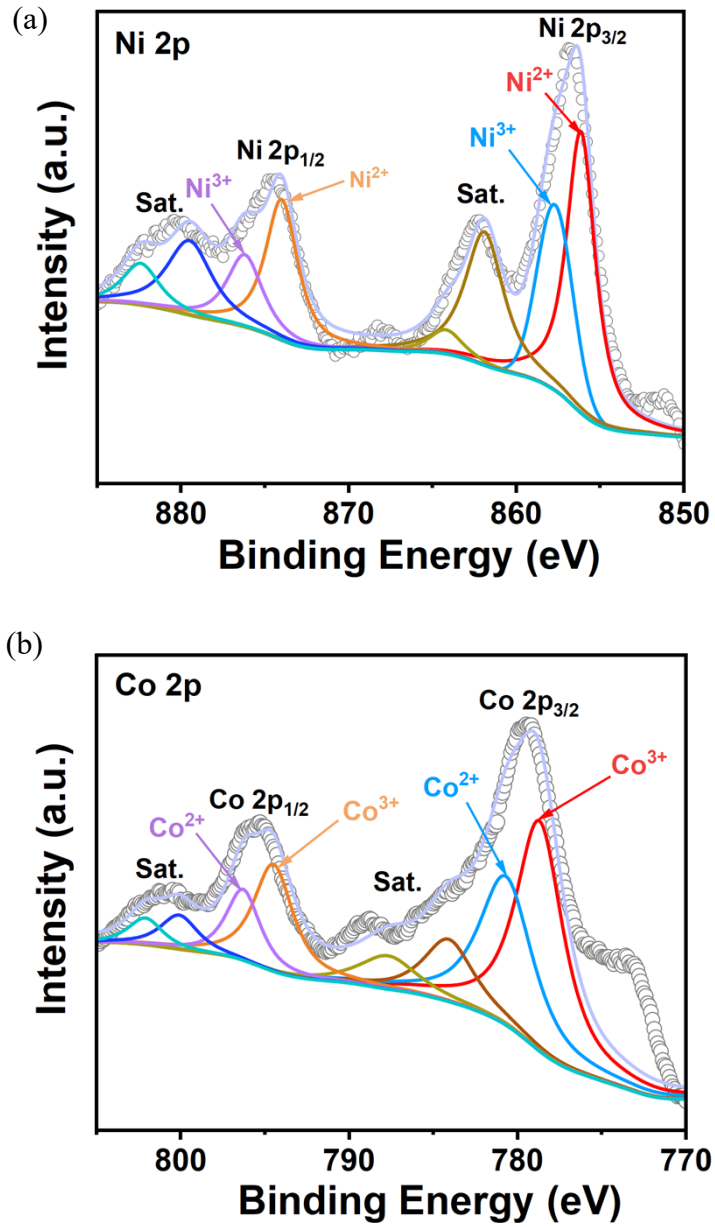

Fig. S7. XPS profiles of (a) Ni 2p for Ni-LDH and (b) Co 2p for Co-LDH.

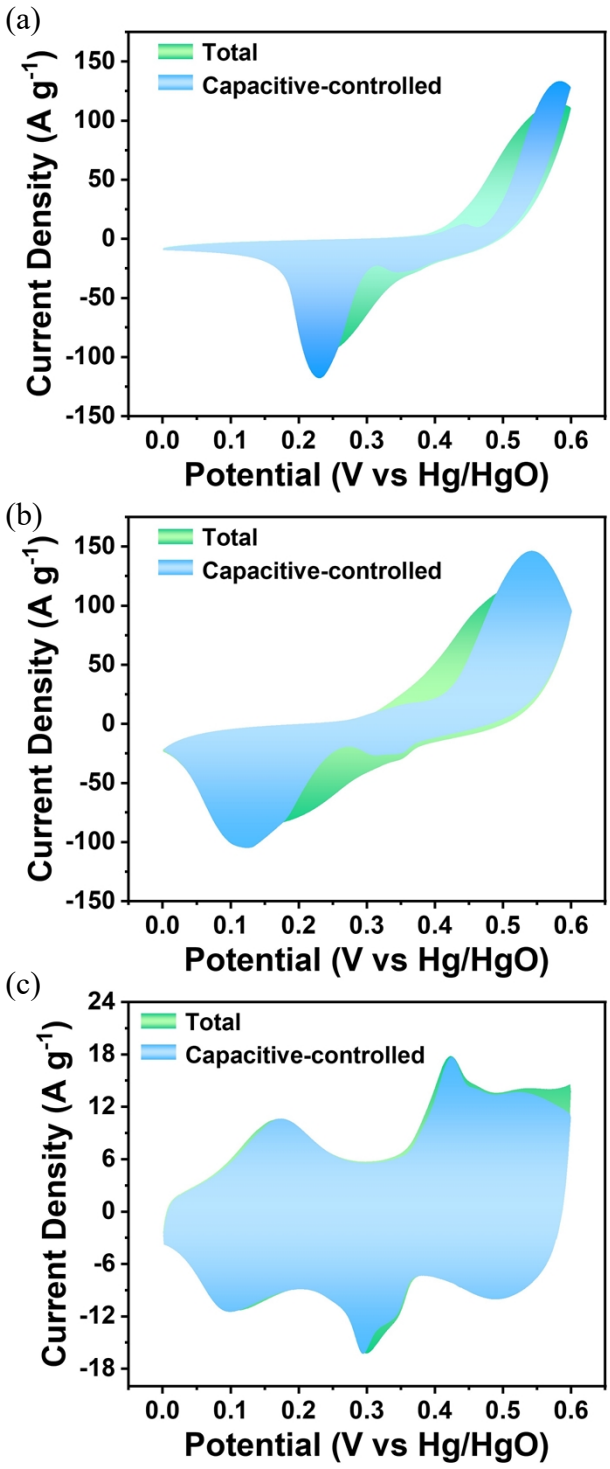

Fig. S8. CV separation of capacitive-controlled capacitance for (a) Ni-LDH, (b) $Ni_{0.7}Co_{0.3}$-LDH, and (c) Co-LDH at 30 mV s^{-1}.

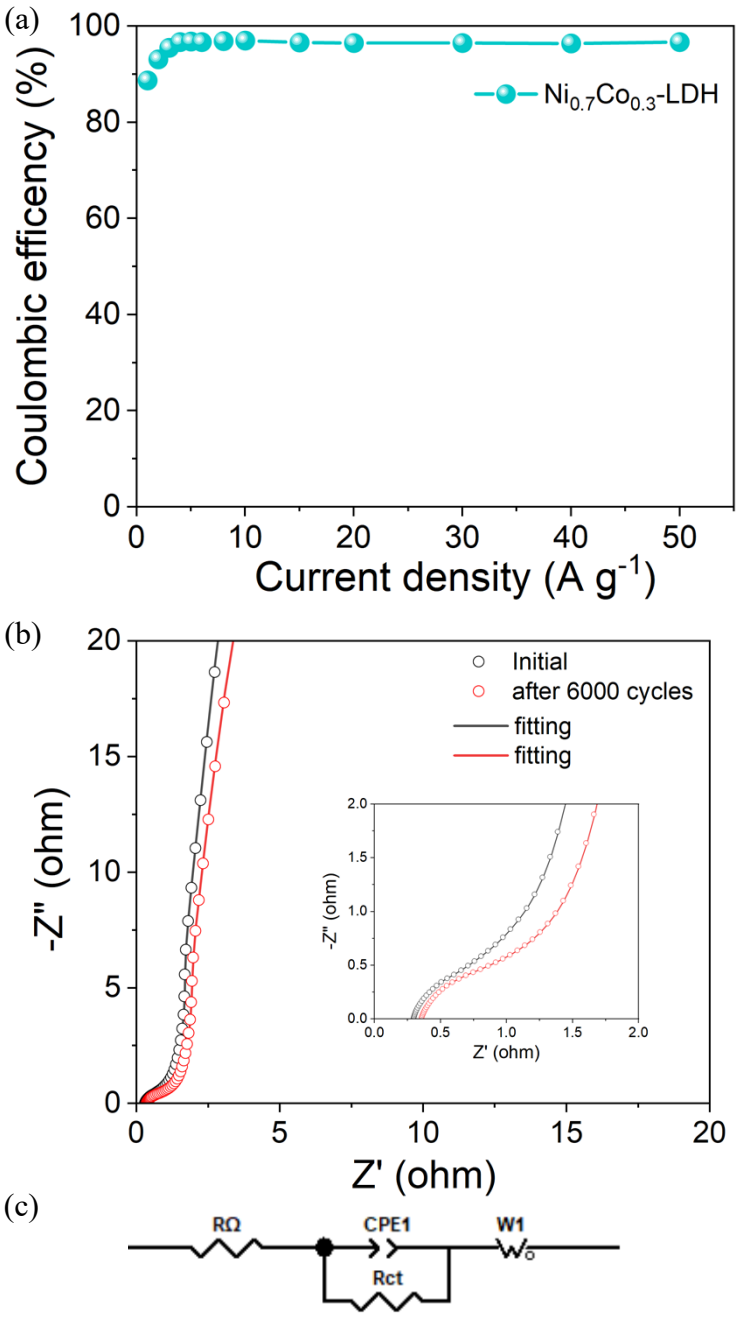

Fig. S9. (a) Coulombic efficiency of $Ni_{0.7}Co_{0.3}$-LDH at various current densities. (b) EIS plots of $Ni_{0.7}Co_{0.3}$-LDH electrode at initial state and after 6000 cycles. (c) Equivalent circuit of EIS fitting.

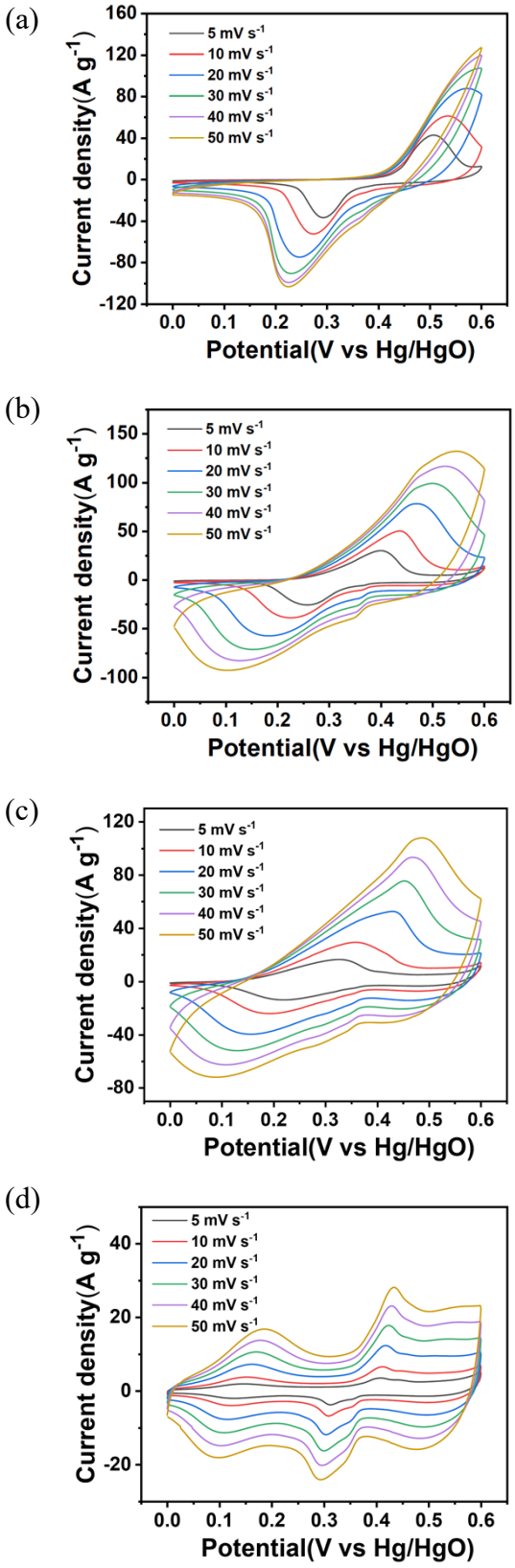

Fig. S10. CV curves of (a) Ni-LDH, (b) $Ni_{0.5}Co_{0.5}$-LDH, (c) $Ni_{0.3}Co_{0.7}$-LDH, and (d) Co-LDH from scan rates of 5 to 50 mV s^{-1}.

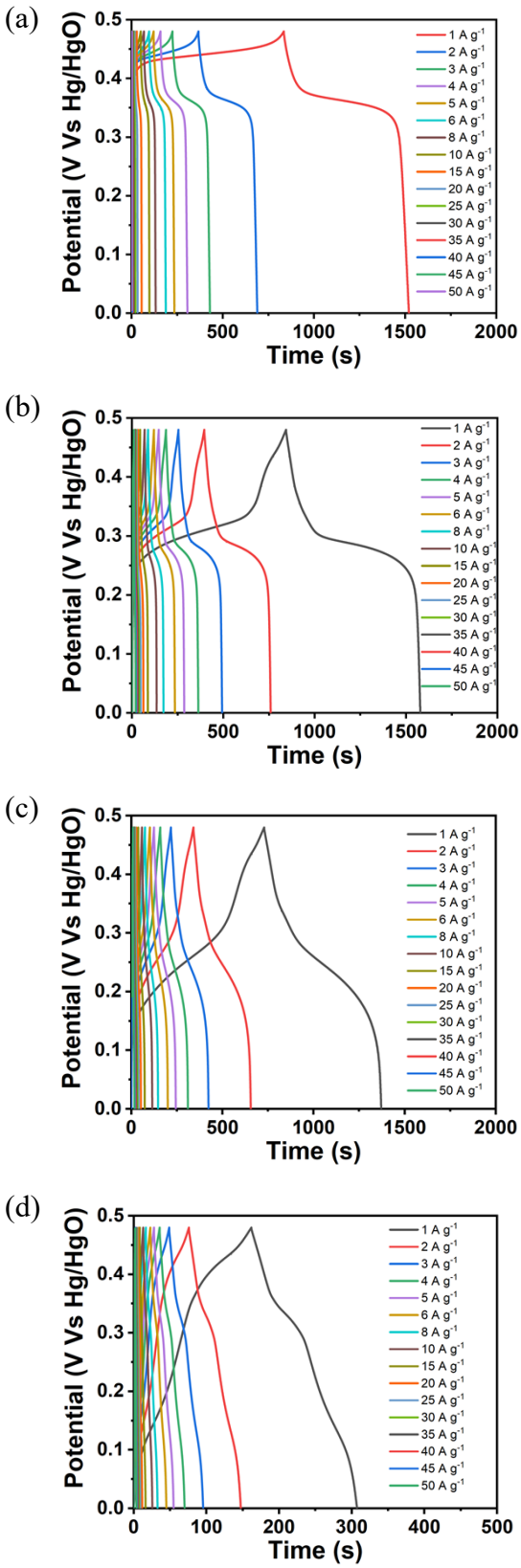

Fig. S11. GCD curves of (a) Ni-LDH, (b) $Ni_{0.5}Co_{0.5}$-LDH, (c) $Ni_{0.3}Co_{0.7}$-LDH, and (d) Co-LDH from current densities of 1 to 50 A g^{-1}.

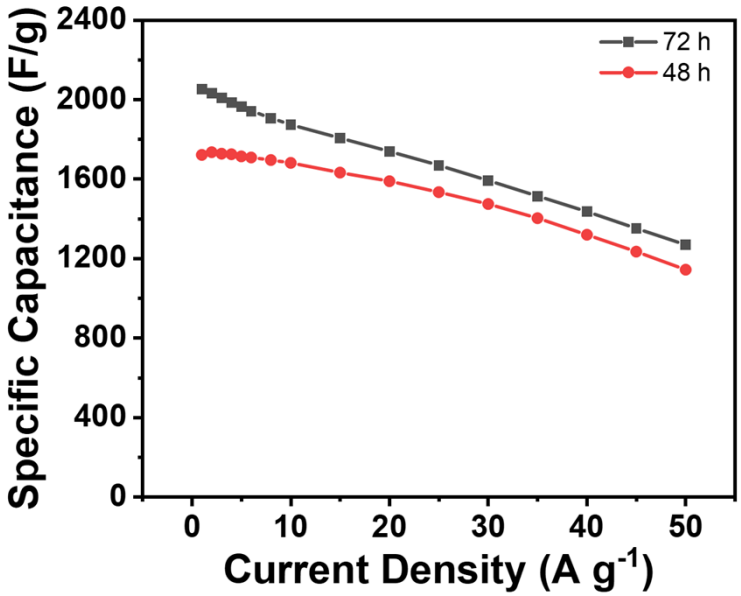

Fig. S12. Rate performances of $Ni_{0.7}Co_{0.3}$-LDHs synthesized in different time.

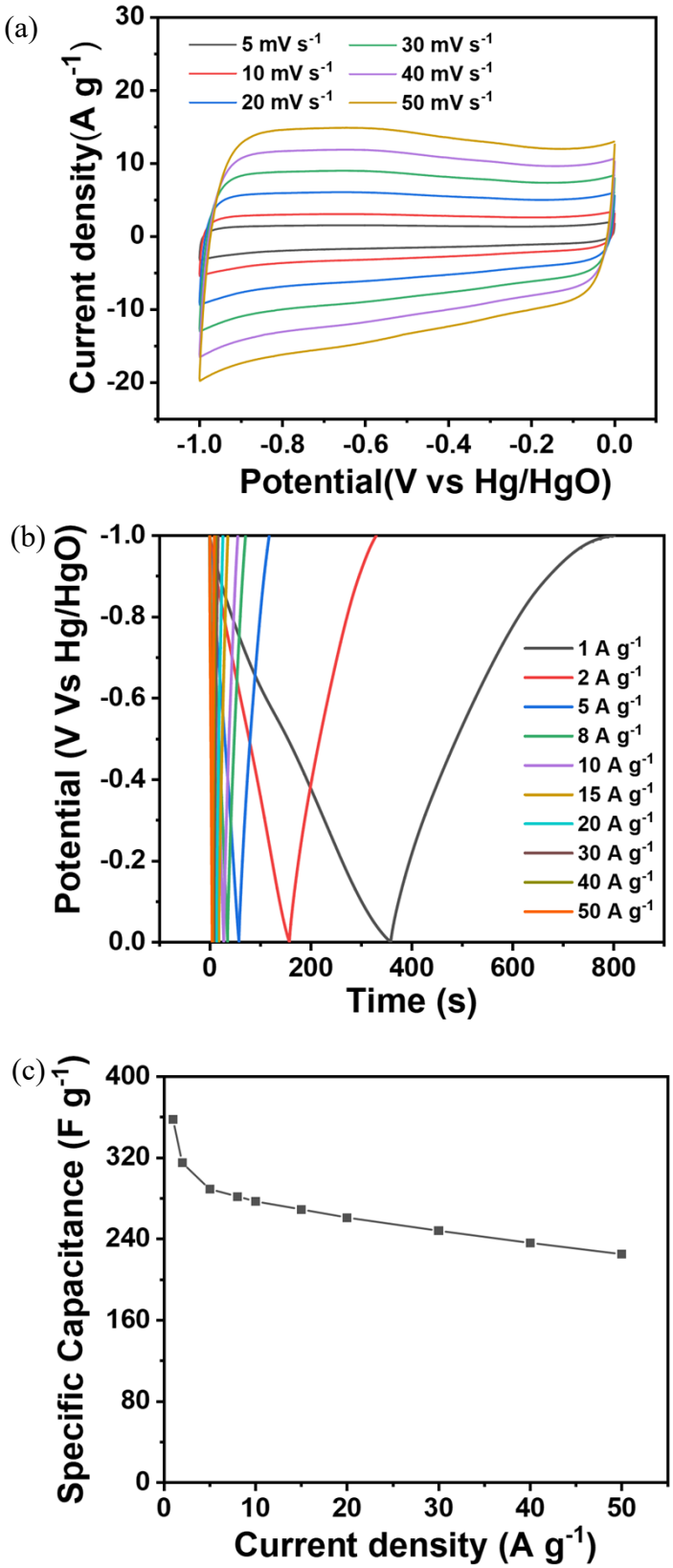

Fig. S13. (a) CV curves from 5 to 50 mV s^{-1}, (b) GCD profiles from 1 to 50 A g^{-1}, and (c) rate performance of AC.

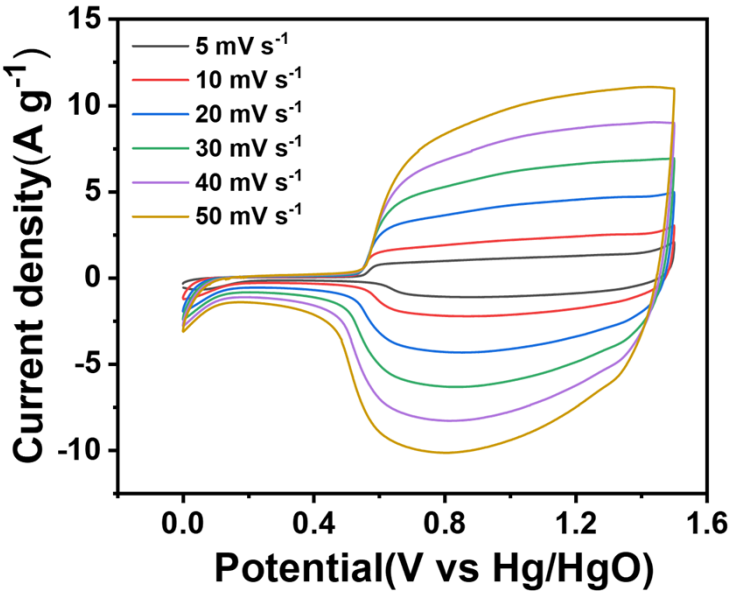

Fig. S14. CV curves of $Ni_{0.7}Co_{0.3}$-LDH//AC ASC.

Table S1. Relative elements ratio of Ni^{2+}/Ni^{3+} and Co^{2+}/Co^{3+} for Ni-LDH, $Ni_{0.7}Co_{0.3}$-LDH and Co-LDH.

Ni-LDH:

valence \ element	Ni 2p 3/2	Ni 2p 1/2	Co 2p 3/2	Co 2p 1/2
+2	63.0%	63.8%	-	-
+3	37.0%	36.2%	-	-

$Ni_{0.7}Co_{0.3}$-LDH:

valence \ element	Ni 2p 3/2	Ni 2p 1/2	Co 2p 3/2	Co 2p 1/2
+2	77.6%	77.9%	38.6%	39.8%
+3	22.4%	22.1%	61.4%	60.2%

Co-LDH:

valence \ element	Ni 2p 3/2	Ni 2p 1/2	Co 2p 3/2	Co 2p 1/2
+2	-	-	42.3%	42.6%
+3	-	-	57.7%	57.4%

Table S2. Internal resistance and contact resistance of NiCo-LDHs.

	Internal resistance (R_{Ω}, Ω)	Contact resistance (R_{ct}, Ω)
$Ni_{0.7}Co_{0.3}$-LDH	0.3014	0.0908
Ni-LDH	0.3503	0.1557
$Ni_{0.5}Co_{0.5}$-LDH	0.3431	0.1335
$Ni_{0.3}Co_{0.7}$-LDH	0.3653	0.1215
Co-LDH	0.3453	0.1351

Table S3. Comparison of specific capacitance and cyclic performance of $Ni_{0.7}Co_{0.3}$-LDH and other reported nickel-based materials.

Sample	Specific capacitance	Rate performance	Cyclic performance (electrode)	Cyclic performance (device)	Reference
$Ni_{0.7}Co_{0.3}$-LDH	2052 F g^{-1} at 1 A g^{-1}	1256 F g^{-1} at 50 A g^{-1}	72% after 6000 cycles	90.8% after 5000 cycles	This article
Ni_3Si_2/NiOOH/G	1193 F g^{-1} at 1 A g^{-1}	350 F g^{-1} at 50 A g^{-1}	-	90.7% after 6000 cycles	*Nano-Micro Lett., 2021, 13, 2*
Ni_xB/Graphene	1822 F g^{-1} at 1 A g^{-1}	1179 F g^{-1} at 20 A g^{-1}	97.5% after 2000 cycles	96% after 2000 cycles	*ACS Nano, 2019, 13, 9376-9385*
$NiCo_2S_4$-G	1036 F g^{-1} at 1 A g^{-1}	705 F g^{-1} at 20 A g^{-1}	87.0% after 2000 cycles	80% after 10000 cycles	*Nat. Commun., 2015, 6, 6694*
$CoNi_2S_4$-G-$MoSe_2$	1141 F g^{-1} at 1 A g^{-1}	580 F g^{-1} at 20 A g^{-1}	108% after 2000 cycles	-	*Adv. Energy Mater., 2016, 6, 1600341*
CoP/NiCoP	1106 F g^{-1} at 1 A g^{-1}	600 F g^{-1} at 100 A g^{-1}	100% after 1000 cycles	95% after 2000 cycles	*Adv. Energy Mater., 2019, 9, 1901213*
Ni-Co-Al-LDH	748 F g^{-1} at 1 A g^{-1}	570 F g^{-1} at 20 A g^{-1}	80% after 5000 cycles	97.8% after 10000 cycles	*ACS Energy Lett., 2018, 3, 132−140*
NiO-Co_3O_4-GQDs	1361 F g^{-1} at 1 A g^{-1}	753 F g^{-1} at 30 A g^{-1}	76.4% after 3000 cycles	-	*J. Mater. Chem. A, 2019, 7, 7800*
CoNi-Pyrophosphates	1259 F g^{-1} at 1.5 A g^{-1}	656 F g^{-1} at 30 A g^{-1}	88.9% after 1000 cycles	80% after 2000 cycles	*ACS Appl. Mater., Interfaces, 2016, 8, 23114-*

					23121
Ni-nCPs	1066.9 F g^{-1} at 1 A g^{-1}	842.7 F g^{-1} at 10 A g_{-1}	58.6% after 3500 cycles	46.4% after 4000 cycles	*Nanoscale, 2021, 13, 11112–11119*

Table S4. Comparison of synthesis methods between $Ni_{0.7}Co_{0.3}$-LDH and other reported nickel-based materials.

Sample	Method	synthesis condition	Reference
Acetate ions-intercalated $Ni_{0.7}Co_{0.3}$-LDH	Solvothermal	120℃, 72h in 20 mL methanol	This work
P, Se-NiCo LDH	Hydrothermal	120℃, 3h in 35 mL DI water	*Mater. Res. Lett.* 2022, 10, 9, 593–601
Ni-Co-Al-LDH	Hydrothermal	150℃, 48h in 50 mL DI water	*ACS Energy Lett., 2018, 3, 132−140*
Mo-doped NiCo-LDH	Microwave method	150°C, 1 h in 30 ml DI water	*Small*, 2023, 2306382
Mn-doped $Ni(OH)_2$	Hydrothermal	100℃, 2h in 60 mL DI water	*Journal of Energy Chemistry*, 2021, 61, 497–506
NiCo-DH@OAC	Hydrothermal	180℃, 12h in 20 mL DI water and 20 mL ethanol	*Chemical Engineering Journal*, 2023, 454, 140280
NiCo-LDH	Solvothermal	180℃, 12h in 4 mL DI water and 32 mL ethanol	*Journal of Colloid and Interface Science*, 2022, 1120–1127
NiCo LDH/$Co(OH)_2$	Hydrothermal	90℃, 6h in 70 mL DI water	*Chemical Engineering Journal*, 2021, 403, 126325

NiFeAl LDHs	Hydrothermal	160℃, 6h in 60 mL DI water	*Journal of Hazardous Materials*, 2021, 404, 124113
NiCo-OOH	Hydrothermal	60℃, 12h in 100 mL DI water	*Chemical Engineering Journal*, 2023, 476, 146638